

# The influence of zinc loadings on the selectivity control of bio-ethanol transformation over MgO-SiO<sub>2</sub> catalysts

Xuefei Wang<sup>a</sup>, Yong Men<sup>a,\*</sup>, Jinguo Wang<sup>a</sup>, Shuang Liu<sup>a</sup>, Qiaoling Song<sup>a</sup>, Mei Yang<sup>b,\*</sup>

<sup>a</sup> College of Chemistry and Chemical Engineering, Shanghai University of Engineering Science, Shanghai, 201620, PR China

<sup>b</sup> Dalian National Laboratory for Clean Energy, Dalian Institute of Chemical Physics, Chinese Academy of Sciences, Dalian, 116023, PR China

## ARTICLE INFO

### Keywords:

Ethanol  
1,3-Butadiene  
Acetaldehyde  
MgO-SiO<sub>2</sub> catalyst  
ZnO loading  
Mg-O-Si interfacial bonds

## ABSTRACT

Catalytic transformation of ethanol has been studied over a series of MgO-SiO<sub>2</sub> composite catalysts with different ZnO loadings. Vast differences in product selectivity are obtained by varying ZnO loadings in enabling the control over product distribution. Our results reveal that MgO-SiO<sub>2</sub> composite catalysts with low ZnO loadings tend to show an enhanced efficiency for C-C bond coupling and exceptionally high selectivity to 1,3-butadiene whereas the high ZnO loadings favor the formation of acetaldehyde *via* dehydrogenation. Thorough analysis of characterization results *via* XRD, BET, IR, TPD, and <sup>29</sup>Si MAS NMR indicates that ZnO loading influences the extent of MgO and SiO<sub>2</sub> interaction during preparation, and the surface acid-base chemistry, which were both found to correlate with the catalytic performance. This study proposes that the Mg-O-Si interfacial structure formed by the strong MgO and SiO<sub>2</sub> interaction at low ZnO loadings is of prime importance for the formation of 1,3-butadiene, benefiting from the desirable properties of balanced dehydrogenation and C-C bond coupling while excess ZnO loadings destroy the Mg-O-Si interfacial bonds over the MgO-SiO<sub>2</sub> composite catalysts, which are the key structures required for C-C bond growth.

## 1. Introduction

Bio-ethanol produced from biomass has emerged as a promising raw material for production of a number of valuable chemical products [1–4], such as acetaldehyde [5], ethylene [6], ethyl acetate [7], and 1,3-butadiene(1,3-BD) [8], which are mainly obtained as by-products of the naphtha cracking process. Bio-ethanol has been extensively studied as a platform molecule for the production of ethylene by acid-catalyzed ethanol dehydration over various catalysts such as alumina [9], zeolites [10] and heteropoly acids [11]. Supported metal catalysts can also selectively transform ethanol into acetaldehyde [12], acetic acid [13] and ethyl acetate [14] depending on the active metals and supports as well as the reaction conditions. Moreover, supported metal catalysts, in particular Ce and Ni with the good ability for deep dehydrogenation and C-C bond scission, have been demonstrated to be excellent catalysts for hydrogen production through ethanol reforming [15–18].

Transformation of bio-ethanol to acetaldehyde and its derivatives C<sub>4</sub>-olefins has been recognized as one of the most important strategic reactions for the production of high value-added chemicals [19–21]. Direct conversion of bio-ethanol into 1,3-BD (Lebedev process, ETB) is quite complex due to the nature of cascade reaction involving many unwanted competitive reactions that produce many by-products such as

butanol, acetaldehyde, diethyl ether, ethyl acetate and ethane [22]. González et al. [23] conducted the experiments where relevant intermediate reaction products were individually fed or co-fed in different ratios with ethanol, and showed that acetaldehyde is a stable intermediate with an important role in 1,3-BD production. MgO-SiO<sub>2</sub> mixed metal oxide is the classic bi-functional catalyst effective for Lebedev reaction. It is generally accepted that the appropriate balance of the surface acidic and basic sites of the catalysts dictate the reaction pathway and the selectivity of the final products [24]. For example, previous studies revealed that MgO-SiO<sub>2</sub> composites prepared by wet-kneading method exhibited the superior catalytic performance [25]. It was illustrated that the optimum of surface acidity/basicity can be obtained to achieve a high 1,3-BD yield by variation of MgO:SiO<sub>2</sub> ratios in wet-kneaded samples [26]. Our recent work highlighted the impact of morphology control on the enhancement of 1,3-BD yield [27]. The unique layered flower-like architectures may facilitate the formation of interfacial Mg-O-Si chemical bond and highly enhanced surface basicity in binary MgO-SiO<sub>2</sub> composite catalysts which are mainly responsible for the superior activity.

It is also a common method that the performance of these catalysts can be greatly enhanced by the addition of a third component, typically a transition metal or metal oxide [28,29]. The choice of the third

\* Corresponding authors.

E-mail addresses: [men@sues.edu.cn](mailto:men@sues.edu.cn) (Y. Men), [yangmei@dicp.ac.cn](mailto:yangmei@dicp.ac.cn) (M. Yang).

<https://doi.org/10.1016/j.apcata.2020.117565>

Received 14 January 2020; Received in revised form 10 April 2020; Accepted 13 April 2020

Available online 18 April 2020

0926-860X/ © 2020 Elsevier B.V. All rights reserved.

component used as a promoter is determined by its dehydrogenation capability. Cu and Ag have been used as metallic promoters to increase the yield of 1,3-BD. Angelici et al. [30] used 1 wt.% of copper loading in Mg:Si = 1:1 (mole ratio) catalyst to get 40 % ethanol conversion and 53 % 1,3-BD selectivity. Dagle et al. [31] showed that a 1 % Ag/4 % ZrO<sub>2</sub>/SiO<sub>2</sub>-SBA-16 catalyst leading to 99 % conversion and 71 % 1,3-BD selectivity. In other studies, metal oxides such as ZnO and Na<sub>2</sub>O were also applied to increase the catalytic activity and selectivity for 1,3-BD. Baerdemaeker et al. [32] reported that due to the suppression effect of ethanol dehydration by Zn<sup>2+</sup>, the combination of Zn and Hf in bimetallic Zn and Hf in silica-supported catalyst resulted in a stable, active, and selective catalyst for butadiene production from ethanol, while Wang et al. [33] found that 2000 ppm Na doped Zn<sub>1</sub>Zr<sub>10</sub>O<sub>x</sub> catalyst gave 47 % selectivity to 1,3-BD at 97 % ethanol conversion. Despite the considerable progress achieved in enhancement of 1,3-BD yield due to metal or metal oxide promoters, the principle for the controllable production of acetaldehyde or desirable 1,3-BD during Lebedev process still remained largely unexplored. Our recent study represented the first report that uncovers the principles for tailoring the selectivity of acetaldehyde or 1,3-BD by tuning the size of nano-gold Au/ZnZr<sub>10</sub>O<sub>x</sub> catalyst [34].

Zinc is a special transition metal, as it was reported to improve availability of Lewis base sites [35,36], and has a good track record on ethanol dehydrogenation [37]. In this work, a series of MgO-SiO<sub>2</sub> (65:35) catalysts with different ZnO loadings were prepared by a simple impregnation method and evaluated for selective ethanol transformation. We showed that how selectivity of this reaction can be tailored towards specific cascade formation of either acetaldehyde or 1,3-BD as major products by controlling amounts of ZnO addition into MgO-SiO<sub>2</sub> (65:35) substrate. The purpose of this work is not only to investigate the effect of different ZnO loadings on the selectivity control of desirable products on Zn-promoted MgO-SiO<sub>2</sub> catalyst, but also to improve the fundamental understandings about the interfacial effect of mixed metal oxide catalysts on ethanol conversion.

## 2. Experimental section

### 2.1. Materials

Magnesium hydroxide, tetraethyl orthosilicate (TEOS) and ammonium hydroxide were purchased from Aladdin Chemistry Co. Ltd. (Shanghai, China), ethanol and zinc nitrate hexahydrate were purchased from Sinopharm group chemical reagent co. LTD (Shanghai, China). All chemicals are used directly without further purification.

### 2.2. Catalyst preparation

SiO<sub>2</sub> was prepared by the procedure reported by Stöber et al. [38]: TEOS was hydrolyzed using an ethanol-water ammonia solution (25:15:3.14 vol./vol.) in a closed vessel by stirring at room temperature for 4 h, followed by centrifugation and thorough washing with ethanol. Then the solid products were dried at 100 °C for 12 h, and calcined at 500 °C for 5 h in air.

MgO-SiO<sub>2</sub> (MgSi) catalysts were prepared with a 65:35 M ratio (based on the results of our recent study) by the procedure reported by Kvisle et al. [39]: Mg(OH)<sub>2</sub> and SiO<sub>2</sub> were mixed at 50 °C for 5 h in water. Then the suspension was stirred constantly and heated at 100 °C to remove excess H<sub>2</sub>O. Finally, the dried solid catalyst was calcined at 500 °C for 5 h in air.

The ZnO promoted MgO-SiO<sub>2</sub> catalysts were prepared by incipient wetness impregnation: the solution of Zn(NO<sub>3</sub>)<sub>2</sub>·6H<sub>2</sub>O (Solute mass was determined by the load) was added to the support material and left to equilibrate for 12 h, then dried at 100 °C for 12 h. Finally, the dried solid was calcined at 500 °C for 5 h in air. The above methods were used to prepare different MgSi catalysts loaded with ZnO of 0.1 wt.%, 0.2 wt.%, 0.4 wt.%, 0.8 wt.%, 1 wt.%, 5 wt.%, as denoted as ZnMgSi-X.

### 2.3. Catalyst testing

The conversions of ethanol to 1,3-BD were conducted in a fixed bed quartz tube reactor at atmospheric pressure. In a typical experiment, 100 mg catalyst was loaded in the middle of 5-mm internal diameter quartz beds. A K-type thermocouple was placed in the middle of the catalyst bed to monitor the reaction temperature. The carrier gas (20 mL/min) carried ethanol to pass over the catalyst to on-line gas chromatography through an evaporator kept at constant temperature (20 °C). The reaction temperature was within the range of 300–500 °C. The effluent gas products were heated above 200 °C to avoid the condensation of condensable species and quantified by an online Shimadzu 2014 Gas Chromatography (GC). The product was analyzed with molecular sieves C13X, Al<sub>2</sub>O<sub>3</sub> column (50 m, 0.53 mm ID, 10 μm), Rt-Q-BOND PLOT column (30 m, 0.32 mm ID, 10 μm) by one TCD and two FID detectors. The catalysts were firstly pre-treated in N<sub>2</sub>/ethanol (20 mL/min) at 300 °C for 0.5 h before reaction. Nitrogen was used as the internal standard for calibration and calculation of GC results. The kinetic study was carried out by the Weisz-Prater criterion to discard any mass transfer limitation [40–43].

### 2.4. Catalyst characterization

The crystalline phases of the samples were identified by X-ray powder diffractions (XRD) using a diffraction meter (D/Max-rB) with Cu-Kα radiation (λ = 1.54056 Å) at room temperature. The scanning rate was 4°/min, the 2θ was from 10° to 80°.

The specific surface area of the material was determined by applying Brunauer-Emmett-Teller (BET) model on a Micromeritics ASAP2460 apparatus. The samples were pretreated for 6 h in nitrogen at 200 °C before analysis.

The Fourier transform infrared spectroscopy (FT-IR) signal of the catalyst was recorded on a Nicolet 380 infrared spectrometer (USA). The sample was pressed into a thin self-supported wafer in KBr and placed in the IR cell. The FT-IR spectra of the catalysts were recorded at room temperature against an air background. FT-IR spectral signals in the wave number range of 4000–400 cm<sup>-1</sup>.

The acidity and basicity of the catalyst were investigated by CO<sub>2</sub>-temperature-programmed desorption (CO<sub>2</sub>-TPD) and NH<sub>3</sub>-temperature-programmed desorption (NH<sub>3</sub>-TPD) on a Micromeritics Autochem II 2920 apparatus. 0.05 g of catalyst was installed in a U-shaped fixed-bed quartz micro reactor. After pretreatment under argon at 500 °C for 1 h, the catalyst was cooled to 100 °C, then a mixture gas 5 % CO<sub>2</sub>(NH<sub>3</sub>)/He (30 mL/min) were applied, followed by flowing in He (30 mL/min) until the base line was stabilized, and heating up to 900 °C at 10 °C/min to induce desorption of CO<sub>2</sub>(NH<sub>3</sub>).

The temperature-programmed desorption of ethanol (ethanol-TPD) was used to study the ethanol to 1,3-BD reaction process. 50 mg catalyst in a U-shaped fixed-bed quartz microreactor treated at 500 °C (ramping rate 10 °C/min) for 0.5 h under flowing 3 % O<sub>2</sub>/He (20 mL/min). Then the sample was cooled to 50 °C, switching to He gas (20 mL/min) for 30 min remove water and impurities from the surface of the material. Ethanol was bubbled in a U-shaped fixed-bed quartz micro reactor until the saturated adsorption of ethanol. The sample was purged by flowing 30 mL/min He for 40 min till stabilization of the baseline. The temperature was then raised to 900 °C (10 °C/min) in a He (30 mL/min) gas atmosphere, and the exhaust gas was connected to the HPR20 online mass spectrometer to determine composition at the same time during the heating process. To analyze the composition, different mass-to-charge ratios (m/e) in the mass spectrometry have been set to follow the law of mass cracking: hydrogen = 2, acetaldehyde = 44, 1,3-butadiene = 54, ethylene = 27.

In order to further study the acid-base properties of the catalysts, the samples were characterized by isopropanol temperature-programmed desorption (IPA-TPD). A quartz U-tube reactor was loaded with 100 mg of sample. The samples were pretreated in the presence of

He with flow of 30 mL/min at 300 °C for 1 h. Subsequently, the sample was cooled to 50 °C and pulse ethanol adsorption was conducted. After saturated adsorption of isopropanol, the sample was then heated to 500 °C with a ramp of 10 °C/min, and the exhaust gas was analyzed by the HPR20 online mass spectrometer. Mass spectrometry can distinguish different products by collecting different charge ratios. The charge/mass ratios are set as follows: isopropanol ( $C_3H_8O$ ) = 45, acetone ( $C_3H_6O$ ) = 43, propylene ( $C_3H_6$ ) = 41.

A Bruker Avance400 spectrometer was used to collect Magic-angle spinning nuclear magnetic resonance (MAS NMR) spectra. The resonance frequency of  $^{29}Si$  is 79.5 MHz in the field of  $^{29}Si$  MAS NMR spectrum. 17,000 scans were accumulated with a recycle delay of 10 s. The spinning frequency of the rotor is 5 kHz. The catalysts were packed in 4 mm zirconia rotors. Tetramethyl silane was used as chemical shift reference.

In this study, the following formula was used to calculate the conversion rate of ethanol and the selectivity of the products, and the carbon balance of all catalysts is greater than 95 %:

$$Conversion = \frac{ethanol_{in} - ethanol_{out}}{ethanol_{in}} \times 100\% \quad (1)$$

$$Selectivity = \frac{x_i n_i}{\sum_z x_z n_z} \times 100\% \quad (2)$$

$$Yield = conversion \times selectivity \times 100\% \quad (3)$$

$x_i$  is the mole fraction of products (i),  $n_i$  is the number of carbon atoms in carbon-containing products (z).

### 3. Results and discussion

#### 3.1. Catalyst characterization

Aiming to detect the interaction between ZnO and MgSi catalysts, the XRD patterns of MgSi catalysts with varying loadings of ZnO were recorded. (Fig. 1). The diffraction peaks at  $2\theta$  of 36.9°, 42.9°, 62.3°, 74.7° and 78.6° was detected, corresponding to diffraction planes of the periclase phase of cubic MgO (111), (200), (220), (311) and (222) [44]. With the addition of ZnO, the XRD intensity of MgO decreased and broadening was observed, indicating a reduction of crystallite size and crystallinity. The diffraction peak of MgO at 43.5° shifts toward lower value indicated that the Zn-promoted catalysts may form a solid solution during the preparation due to  $Zn^{2+}$  incorporation into the  $Mg^{2+}$  lattice [37]. The ZnMgSi-10 catalysts displayed well-resolved diffraction peaks around  $2\theta$  of 31.7°, 34.4°, 36°, 56° (Fig. S1), indicative of the

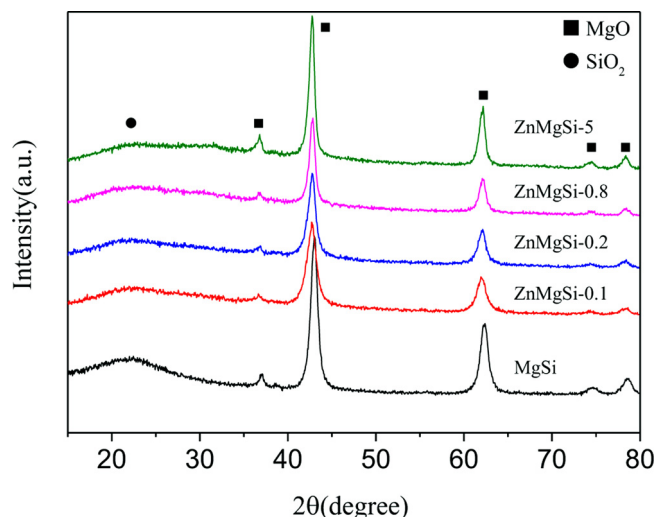


Fig. 1. XRD patterns of ZnMgSi-X catalysts.

**Table 1**  
Textural properties of ZnMgSi-X mixed oxides determined by  $N_2$  adsorption and XRD.

Samples	$S_{BET}$ ( $m^2/g$ )	$V_p$ ( $cm^3/g$ )	$D_p$ (nm)	Crystallite size(nm)
MgSi	87	0.53	17.9	12.4
ZnMgSi-0.1	75	0.33	21.1	12.3
ZnMgSi-0.2	48	0.32	27.8	11.4
ZnMgSi-0.8	34	0.24	28.6	11.0
ZnMgSi-5	31	0.24	29.9	10.5

(100), (002), (101) and (110) facets, respectively, in the bulk phase ZnO (JCPDS Card No. 36-1451). No diffraction peaks of ZnO species could be observed over the samples with ZnO loading lower than 5 wt. % owing to the low Zn loading or its presence in form of highly dispersed state on the catalyst surface. Meanwhile, the broad peaks between 20°–40° found in all samples were attributed to the presence of amorphous silica. No other phases were identified by XRD patterns, in accordance with Angelici et al. [30]. Similar results have also been observed by Larina [45] and Taifan [37].

Table 1 collected the physical structure parameters of the catalysts obtained from XRD patterns and nitrogen adsorption isotherms (Fig. S2). As illustrated in Fig. S2, all the samples displayed the typical type IV isotherms with H3 hysteresis loops in the relative pressure ( $P/P_0$ ) range from 0.4 to 1.0, which is associated to narrow slit pores. The corresponding pore size distribution curves in Fig. S2 indicated that the micropore structure of MgSi sample. The loading of ZnO into MgSi matrix eliminates considerably the micropore due to the interaction of Zn species and MgO within the micropores MgSi and creates mesoporous structure. As can also be seen in Table 1, BET surface areas and pore volumes of composite oxide catalysts varied significantly in the range of 87–31  $m^2/g$  and 0.53–0.24  $cm^3/g$ , respectively, indicating a strong influence of the ZnO loadings on the textural properties. It was found that the specific surface area of all the catalyst decreased with the increasing ZnO loadings along with the decreased crystal size of MgO. Loading ZnO into MgSi leads to the loss of crystallization and the microporous structure due to the decreased crystal sizes, thus decreasing the surface area. The incorporation of Zn into the MgO lattice could be responsible for the collapse of micropore structure leading to a decrease in surface area. Meanwhile, the pore volumes of all ZnMgSi catalyst decreased with the increase of ZnO loadings, probably due to the enhanced pore blockage caused by excessive ZnO loading.

Fig. 2 shows FT-IR spectra for the various samples in the region of 4000–400  $cm^{-1}$ . The FT-IR spectra of MgSi catalysts were similar to that reported in the literatures [30]. The ZnMgSi catalysts show similar

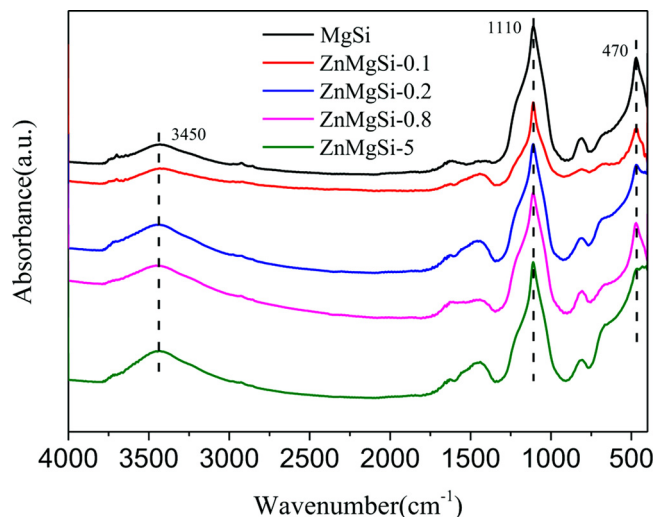


Fig. 2. FT-IR spectra of the ZnMgSi-X catalysts.

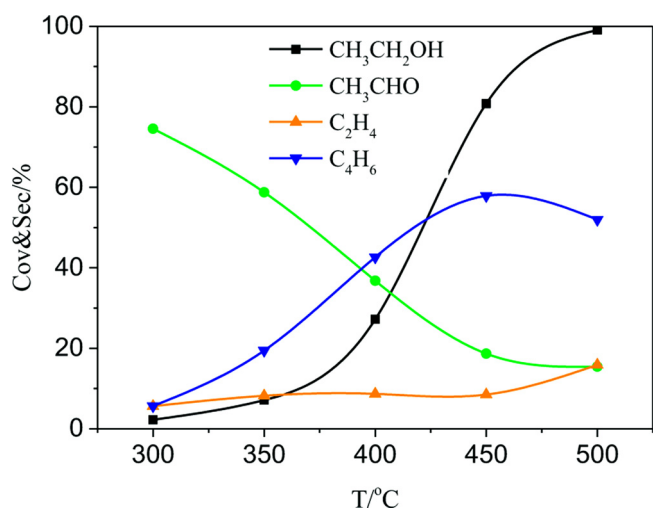


Fig. 3. Temperature-dependent reactivity of the ZnMgSi-0.2 catalyst.

spectral features to these in the MgSi catalysts, illustrating two obvious sharp absorption bands at  $1110\text{ cm}^{-1}$  and  $3450\text{ cm}^{-1}$ , respectively, while the former is the stretching vibrations of the hydroxyl groups of water physically adsorbed on the surface and the latter can be assigned to the asymmetric Si–O–Si stretching mode. Moreover, depending on the ZnO loadings, some obvious changes have been noted on the absorption feature located at  $470\text{ cm}^{-1}$  belonging to the stretching vibration of Mg–O–Si bonds [25]. In particular, this feature weakened due to the introduction of ZnO and almost vanished at the high ZnO loading of 5 wt.%. In our previous work, Mg–O–Si bonds have been proposed to be the crucial active structure for the selective production of 1,3-BD from ethanol [26]. The observed decrease in magnesium silicates catalyst by Taifan et al. [37] has been ascribed to broken Mg–O–Si linkages due to the interaction of Zn with Mg–O–Si upon Zn addition. Our result suggests that Zn interacts strongly with the OH group and plays a key role in change of the Mg–O–Si structure.

### 3.2. Catalytic activity

The effect of reaction temperature on ETB reactivity is investigated over ZnMgSi-X catalysts. Fig. 3 displays the catalytic performance of the ZnMgSi-0.2 catalyst for ethanol to 1,3-BD at WHSV of  $1.63\text{ h}^{-1}$ , and ethylene, acetaldehyde and 1,3-BD are detected as the main products in the catalytic process. As the temperature increases, the ethanol conversion rate increases gradually, while the product distribution is found to be dependent on the reaction temperature. The selectivity of acetaldehyde decreased gradually, and that of 1,3-BD increased. The increase of ethylene selectivity at the expense of decreasing acetaldehyde selectivity observed in the investigated temperature range suggests that ethanol dehydration and dehydrogenation are two parallel competitive reactions. Moreover, volcano-like 1,3-BD selectivity along with the continuously decreased acetaldehyde selectivity indicates that the acetaldehyde formed *via* ethanol dehydrogenation is the primary product of ethanol transformation, whereas 1,3-BD is a secondary product in the cascade reaction sequences.

In order to understand the impact of catalyst composition on the activity, the effect of Zn addition was investigated over the ternary ZnMgSi catalysts with various Zn loadings. Fig. 4 compares the product distribution for ethanol conversion over catalysts with different ZnO loadings at  $450^\circ\text{C}$ . Ethylene, acetaldehyde and 1,3-BD are detected as the main products in the catalytic process over MgSi substrate. More details about the selectivity of all detectable products over the catalysts can be found in Table S1. On one hand, the rate of ethanol conversion is found to increase with increasing ZnO loading. On the other hand, the product selectivity of the reaction was highly dependent on the loading

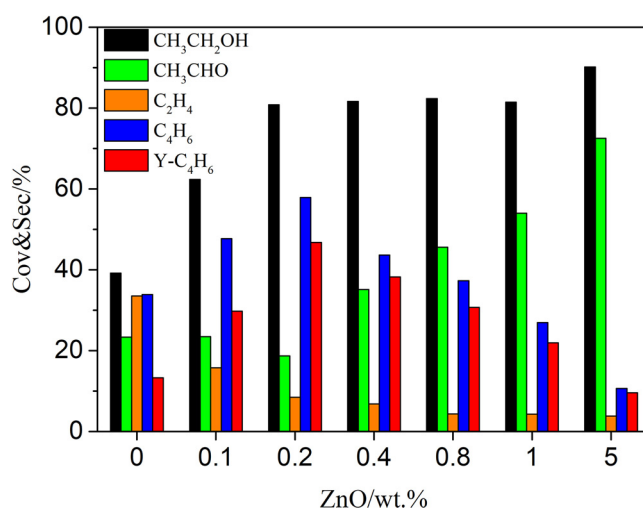


Fig. 4. Product distribution of ethanol conversion over ZnMgSi-X catalysts.

of ZnO, demonstrating pronounced effects of varying ZnO loadings on the selectivity control of ethanol transformation in this catalyst system. Interestingly, addition of ZnO to MgSi catalyst suppressed the formation of undesired byproduct ethylene, suggesting that Zn sites are responsible for the inhibition of ethylene formation *via* dehydration. When MgSi is doped with 0.1 wt.% ZnO, significantly enhanced 1,3-BD selectivity is observed along with the enhanced ethanol conversion rate. An increase in the ZnO loading to 0.2 wt.% resulted in the highest catalytic activity for C4 olefin, *i.e.* the 80 % ethanol conversion and 58 % 1,3-BD selectivity with the lowest acetaldehyde of 16 %. Notably, 1,3-BD selectivity started to decrease with further increase of ZnO loading while acetaldehyde selectivity increased continuously, indicating that the excess ZnO loadings disable the catalytic functionality of the key structure required for C–C bond growth.

The stability of ZnMgSi-0.2 catalyst was studied, and the results are shown in Fig. 5. The conversion rate of ethanol decreases gradually within 50 h from 80 % to 55 % and 1,3-BD selectivity declined slowly from 58 % to 55 %, while the selectivity of acetaldehyde and ethylene retained almost unchanged. Based on literatures [33,37,46] and our thermogravimetric results performed over spent sample (Fig. S3), the deactivation of ZnMgSi catalyst may be mainly associated with the surface basic sites for secondary acetaldehyde to 1,3-butadiene.

To shed further light on the origin of Zn-loading dependence on the

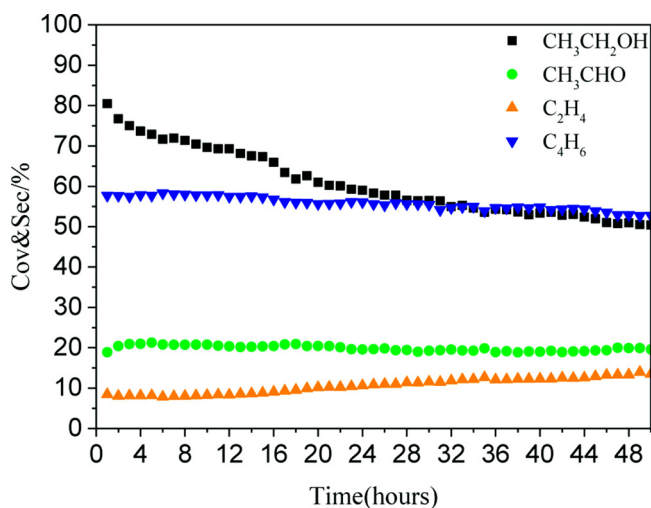


Fig. 5. Stability test of the ZnMgSi-0.2 catalyst. Conditions: 0.1 g of catalyst, ethanol (gas phase) molar fraction 5.79 vol.%, N<sub>2</sub> flow rate = 20 mL/min, T =  $450^\circ\text{C}$ , respectively.

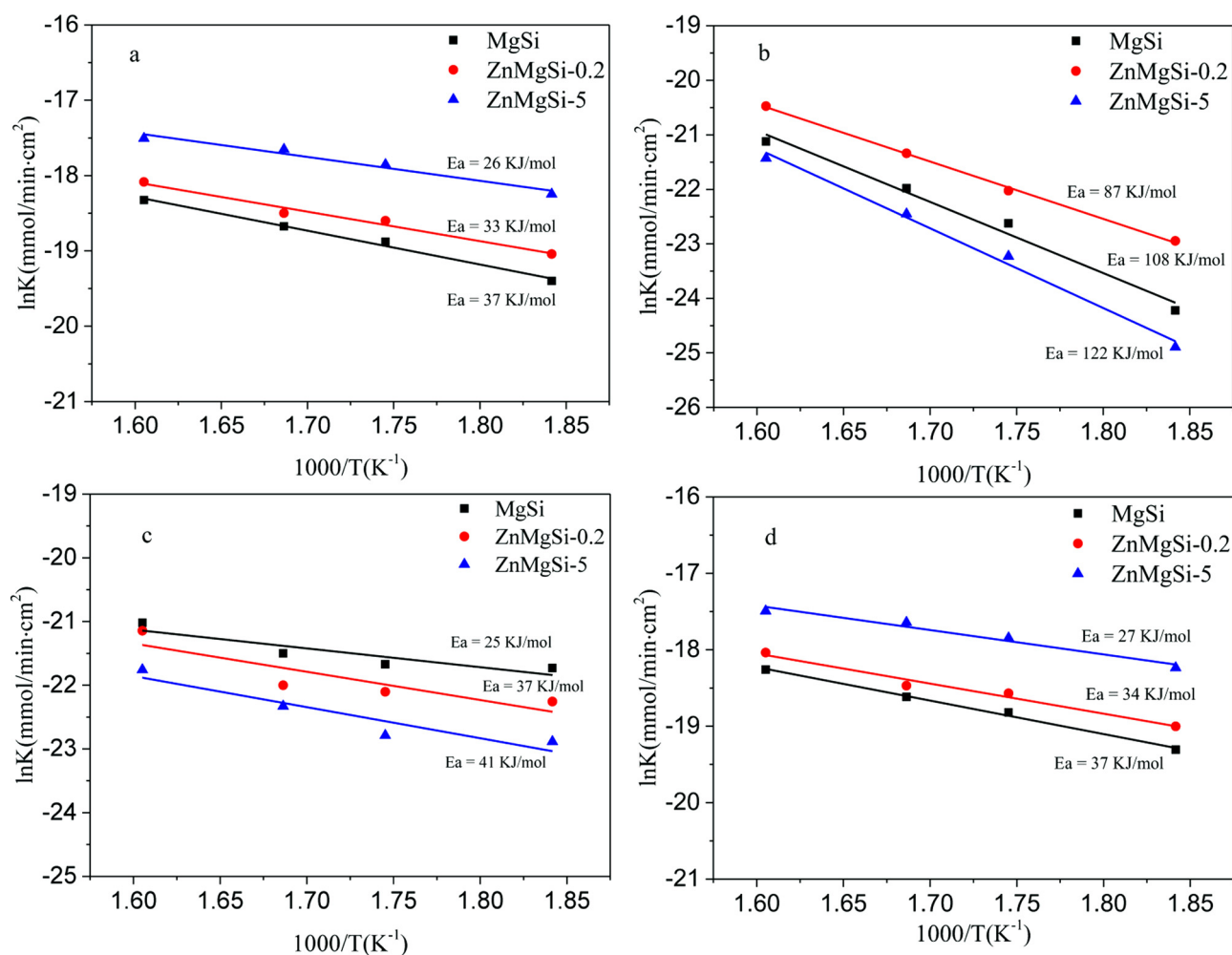


Fig. 6. Arrhenius-type plots of production rate over the MgO-SiO<sub>2</sub> catalysts with different ZnO loadings (a, acetaldehyde b, 1,3-butadiene c, ethylene d, ethanol).

selectivity control of ethanol transformation, the respective activation energy of the key products of acetaldehyde and 1,3-BD were obtained by performing the reaction under the kinetically controlled regime. As shown in Fig. 6, our kinetic study indicates that the difference of the activation energy is the key selectivity descriptor, in consistent with previous studies [34,47]. Over the catalyst without Zn, the activation energies of acetaldehyde and 1,3-BD were determined to be 37 and 108 kJ/mol, respectively. Over the catalysts with low ZnO loading of 0.2 wt.%, the activation energy of acetaldehyde was slightly lower than that without ZnO, however, the activation energy of 1,3-BD formation became significantly lower than that on the binary catalyst. A further increase of ZnO loading to 5 wt.% resulted in a dramatic increase of activation energy for 1,3-BD formation along with a considerable decrease in activation energy for acetaldehyde generation, leading to preference for the acetaldehyde formation. It was also observed in the Arrhenius-type plots of ethylene in Fig. 6c that a continuous increase of ZnO loading to 5 wt.% resulted in an increase of activation energy for ethylene formation along with a considerable decrease in activation energy for acetaldehyde generation, meanwhile the activation energy of ethanol conversion rate (Fig. 6d) decreased significantly with the increase of ZnO loadings, leading to a highly enhanced reaction rate of ethanol conversion. As a consequence, the product selectivity can be controlled by tuning the ZnO loadings over MgSi.

### 3.3. Structure-activity relationship of catalysts

The inherent acid-base function of the catalysts is an important

factor affecting the catalytic activity [24]. In our previous works [21,26,48], the proper balance of acid-base sites has been thought to be critical to determine the reaction pathway of ethanol conversion and the activity of the catalyst. The acid-base distribution and the number of acid-base sites can be quantitatively analyzed by NH<sub>3</sub>- and CO<sub>2</sub>-TPD over a temperature range of 100–500 °C (Fig. 7). All results desorption results are shown in the Table 2. The binary MgSi catalyst displayed one broad desorption peak of NH<sub>3</sub> centered at 210 °C, assignable to moderate acidic sites. With the addition of ZnO, this desorption peak decreased and shifted toward lower temperature, indicating the appearance of new weak acid sites. The fewer acid sites derived from the reduced peak strength can be related to the generation of byproduct ethylene because ethylene formation are more favorable over the acid site of the catalyst [49]. A further increase of ZnO loading to 5 wt.% resulted in a dramatic decrease of weak acidic site with a considerably lowered moderate acidic sites. Obviously, the addition of Zn significantly can passivate the acidic site of the catalyst surface. By the contrary, there is no new desorption peak in CO<sub>2</sub>-TPD absorption with the ZnO addition, and only one weak base desorption peak and one moderate base absorption peak. The acid-base ratio presents an interesting parameter. Apparently, the addition of zinc oxide increased considerably the available surface basic sites and thus decreased the relative ratio of acid-base sites, suggesting the increased surface basicity. The changes on the surface acid-base properties can be further correlated with the variation of products selectivity. Previous study [50] also reported the similar observation, suggesting that acidic sites are important factors in the conversion of ethanol to ethylene, while the

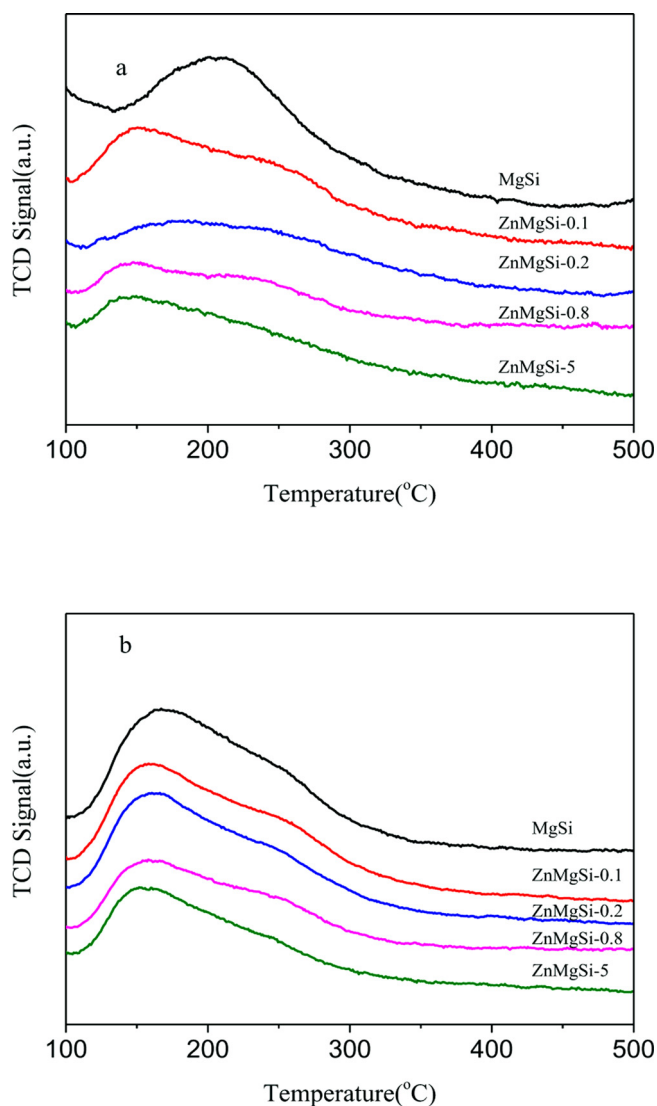


Fig. 7.  $\text{NH}_3$ -TPD (a) and  $\text{CO}_2$ -TPD (b) profiles for the ZnMgSi-X catalysts.

**Table 2**  
Amount of acidic and basic sites for the different ZnMgSi-X catalysts.

Samples	Number of acidic sites ( $T_a$ ) <sup>a</sup> (mmol/cm <sup>2</sup> )	Number of basic sites ( $T_b$ ) <sup>b</sup> (mmol/cm <sup>2</sup> )	$T_b/T_a$	Acetone/Propylene <sup>c</sup>
MgSi	40.5	68.8	1.7	2.8
ZnMgSi-0.1	39.9	78.6	2.0	–
ZnMgSi-0.2	20.5	97.7	4.8	4.2
ZnMgSi-0.8	19.7	103.7	5.3	–
ZnMgSi-5	11.5	112.3	9.8	4.4

<sup>a</sup> Number of acid sites is quantified by  $\text{NH}_3$ -TPD.

<sup>b</sup> Number of basic sites is quantified by  $\text{CO}_2$ -TPD.

<sup>c</sup> Number of acetone/propylene sites is quantified by IPA-TPD.

basic sites provide a driving force for the dehydrogenation of ethanol to acetaldehyde, and the eventual 1,3-BD production from ethanol can only be achieved with an appropriate ratio of acid-base sites.

Ethanol-TPD experiments were carried out over a chemisorption instrument coupled with mass spectrometry [17,51] to explore the interaction of ethanol molecule with the surface of MgSi, ZnMgSi-0.2, and ZnMgSi-5. As shown in the Fig. 8, the main desorption species were identified to be  $\text{H}_2$ ,  $\text{CH}_3\text{CHO}$ ,  $\text{C}_2\text{H}_4$  and  $\text{C}_4\text{H}_6$  (1,3-BD). Analysis of desorbed products in gas phase showed differences between the

catalysts depended on the presence of Zn on the catalyst surface. Two distinct  $\text{H}_2$  peaks were observed over MgSi catalyst, and centered at low temperature of 150 °C and high temperature of 350 °C, respectively. These two  $\text{H}_2$  peaks were attributed to the dehydrogenation of adsorbed ethanol on the catalyst surface, as evidenced by the  $\text{CH}_3\text{CHO}$  desorption peaks in the same temperature range. Evidently, the  $\text{H}_2$  and  $\text{CH}_3\text{CHO}$  desorption peaks at high temperatures were shifted toward lower temperatures on the samples with ZnO, suggesting that the increase of ZnO loadings facilitated the hydrogen production via ethanol dehydrogenation, as shown in Fig. 8a and b. It was also observed in Fig. 8c that ethanol dehydration occurred competitively with its dehydrogenation on MgSi catalyst surface. The relative ratio of  $\text{CH}_3\text{CHO}$ ,  $\text{C}_2\text{H}_4$ , 1,3-BD in the total desorbed carbon species are calculated by deconvoluting the peaks in Fig. 8 and presented in Table S3. As shown in Table S3, the relative ratio of  $\text{CH}_3\text{CHO}$ ,  $\text{C}_2\text{H}_4$  and 1,3-BD were largely dependent on the loading amounts of Zn in MgSi catalysts. The addition of Zn effectively passivated the surface acidic sites and resulted in dramatically decreased ethylene selectivity via ethanol dehydration. Moreover, small amounts of ZnO loading favored a highly enhanced 1,3-BD yield while high loadings of Zn inhibited the aldol condensation step and resulted in poor 1,3-BD yield (Fig. 8d). It is concluded that the variations in the Zn loadings amounts on the catalyst surface may have great impact on the surface adsorbed/desorbed species and the control over their stabilized gaseous products [52]. The results obtained by ethanol-TPD can be well correlated with the reactivity data in this study.

Adsorption and desorption of isopropanol has long been considered as a chemical probe reaction for surface acid–base properties. Therefore, the temperature-programmed desorption (TPD) was carried out to probe the modification of surface acidity and basicity by ZnO addition (Fig. 9). Isopropanol tends to dehydrate to propylene over surface acidic site, and isopropanol tends to dehydrogenate to form acetone on surface basic site [53]. Therefore, the alteration of surface acid–basic strength on the catalyst surface can be determined by relative ratio of desorbed propylene and acetone. As shown in Table 2, the relative ratio of MgSi, ZnMgSi-0.2, and ZnMgSi-5 catalysts were determined to be 2.8, 4.2 and 4.4, respectively, showing a up tendency trend. With the small amount of ZnO addition, the catalytic dehydration activity of ZnMgSi-0.2 is much reduced with respect to MgSi sample while the catalytic dehydrogenation activity is markedly facilitated with the increasing surface basicity, as evidenced by the chemisorption data. A further increase of ZnO loading led to highly enhanced dehydrogenation reactivity, accompanying with the increased surface basicity. The IPA-TPD study confirms that the surface acidity of the MgSi sample is considerably passivated by the ZnO addition, resulting the amount of produced propylene is significantly decreased. The results of IPA-TPD can be well correlated with the results of  $\text{NH}_3$  and  $\text{CO}_2$ -TPD.

In order to better understand the effect of ZnO addition on interfacial Mg–O–Si chemical bonds and catalytic activity, the  $^{29}\text{Si}$  MAS NMR was used to explore the chemical environment around Si. The  $^{29}\text{Si}$  MAS NMR spectra of ZnMgSi catalysts with different proportions are shown in Fig. 10. It is known in  $^{29}\text{Si}$  MAS NMR spectra that the strength of  $^{29}\text{Si}$  MAS NMR signal depends on the density of  $^1\text{H}$  around the  $^{29}\text{Si}$  core and the distance between  $^1\text{H}$ – $^{29}\text{Si}$ , and therefore, a higher  $^{29}\text{Si}$  MAS NMR signal strength predicts shorter distances and greater density of  $^1\text{H}$  around the  $^{29}\text{Si}$ . Obviously, some strong signals appear at –113 ppm, –103 ppm, –92 ppm, –80 ppm, and –75 ppm. The three catalysts with different components generally showed the subtle but the clear differences within the chemical shift from –75 ppm to –100 ppm. It was noted that pure MgSi catalysts showed only one peak of –75 ppm. With the addition of ZnO, the intensity of this broad peak started to decrease at –75 ppm, meanwhile new broad peaks emerged at –80 ppm and at –92 ppm, representing a minor ringwoodite component and siloxane groups [54,55]. According to previous literature reports [25,56], three broad signals at –113 ppm, –103 ppm, –92 ppm are

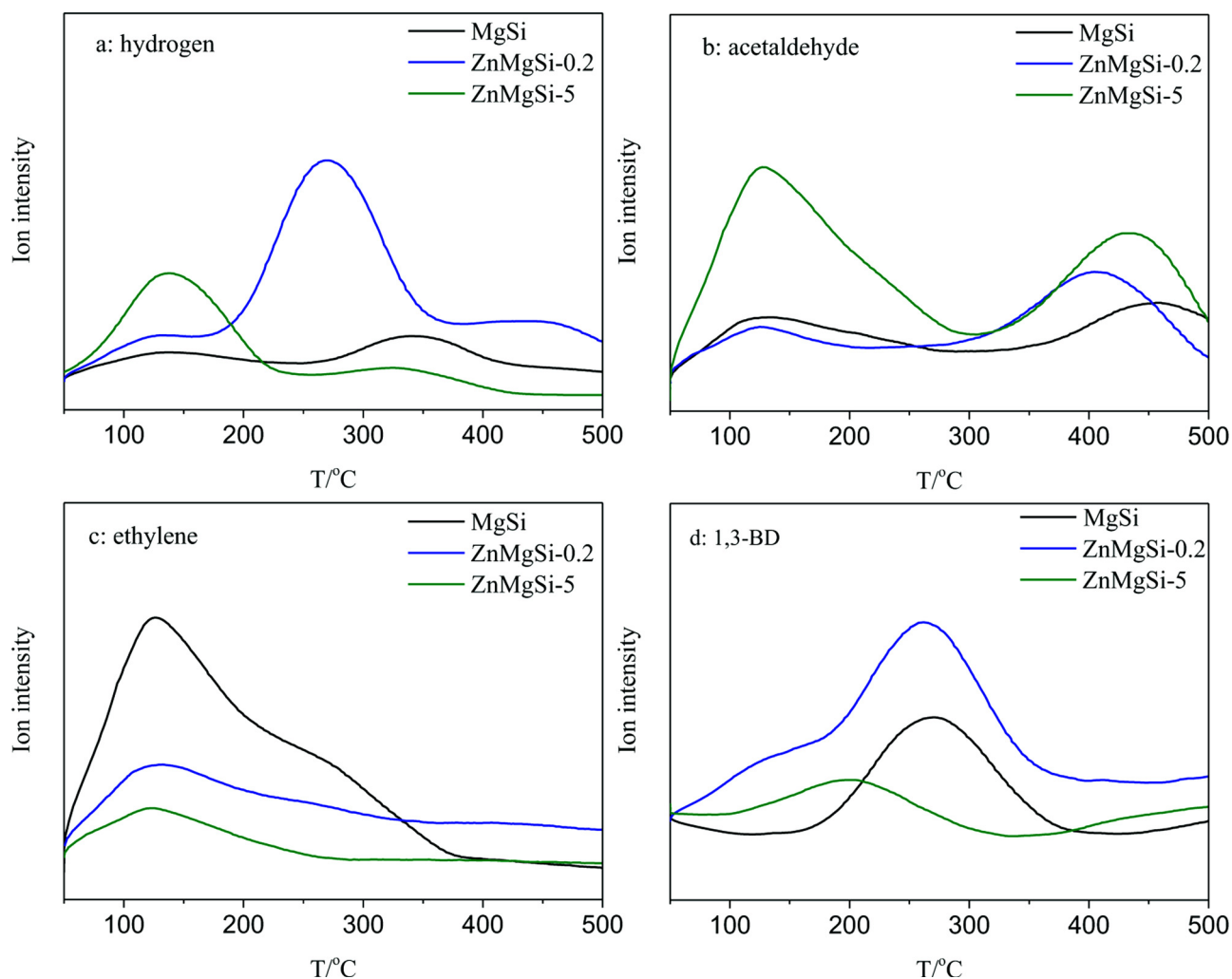


Fig. 8. Ethanol-TPD profiles over ZnMgSi-X catalysts. (m/e: a, hydrogen = 2 b, acetaldehyde = 44 c, ethylene = 27 d, 1,3-BD = 54).

attributed to siloxane groups ((SiO)<sub>4</sub>-Si), simple silanol ((SiO)<sub>3</sub>-Si-OH), and geminal silanol ((SiO)<sub>2</sub>-Si-(OH)<sub>2</sub>), indicating the presence of unreacted SiO<sub>2</sub>. The broad minor ringwoodite component showed up at -80 ppm. -75 ppm is attributed to Si\*(OMg)<sub>2</sub>(OSi)<sub>2</sub>, which are the characteristic signs of Mg-O-Si interfacial bonds. Combining previous FT-IR spectra, we may have a reasonable conclusion. With the small amount of Zn addition, Zn is atomically dispersed in replacement of Mg in Mg-O-Si interfacial structures (Si\*(OMg)<sub>2</sub>(OSi)<sub>2</sub>), and the chemical environment near Si in particular the surface basicity has been altered by the intervention of zinc. Nevertheless, small amounts of zinc do not lead to the great destruction of the Si\*(OMg)<sub>2</sub>(OSi)<sub>2</sub> interfacial bonds, and the catalyst still retains the key interfacial structures required for C-C bond growth. After loading 5 wt.% ZnO onto MgSi catalyst, the excess ZnO loadings destroy the Si\*(OMg)<sub>2</sub>(OSi)<sub>2</sub> interfacial bonds over the MgSi composite catalysts, which are the key structures required for C-C bond growth. Mg-O bonds break off from their original structure and some of Mg-O bonds recombined with Si atoms to form ringwoodite component. Furthermore, (SiO)<sub>2</sub>-Si-(OH)<sub>2</sub> is a combination of hydroxyl radical and Si-(OSi)<sub>2</sub> which is Si\*(OMg)<sub>2</sub>(OSi)<sub>2</sub> bonds after Mg-O bond have separated. The results of <sup>29</sup>Si MAS NMR can be well correlated with the results of FT-IR spectra.

Correlating with the results of TPD, the variation of surface acid-base ratios and acetone/propylene ratios reveal that the addition of Zn passivated the acidic sites and suppressed significantly the surface acidity on the catalyst surface. Moreover, the addition of small amounts

of Zn offered more basic sites, making the surface reaction on the catalyst more favorable for acetaldehyde via ethanol dehydrogenation, which is a key intermediate for 1,3-BD formation. Our results are in good agreement with the recent theoretical DFT prediction made by An [57] and experimental work by Resasco [58] who showed that strong basic sites are beneficial to C-C bond growth via aldol-condensation. The product selectivity toward either acetaldehyde or 1,3-BD formation can be related to the Mg-O-Si interfacial structure. It was noted that Mg-O-Si interfacial structures remained almost intact with a small amount of Zn addition, while the destruction of Mg-O-Si interfacial bonds by 5 wt.% Zn addition is very obvious from the FT-IR and <sup>29</sup>Si MAS NMR spectra. The excess ZnO loadings destroy the Mg-O-Si interfacial bonds over the MgSi composite catalysts, which are the key structures required for C-C bond growth, leading to stabilized formation of acetaldehyde with selectivity of 78 % and the dramatically lowered 1,3-BD yield in the product effluents.

#### 4. Conclusions

In this work, a series of catalysts with different zinc loadings were prepared by a simple impregnation method and evaluated for ethanol transformation. It was found that MgSi with a low loading of Zn (< 0.2 wt.%) exhibited an enhanced 1,3-BD selectivity. A further increase of Zn loading led to the considerably enhanced acetaldehyde selectivity. Multiple characterizations have shown that a highly dispersed zinc oxide species were predominant in the MgSi samples of low

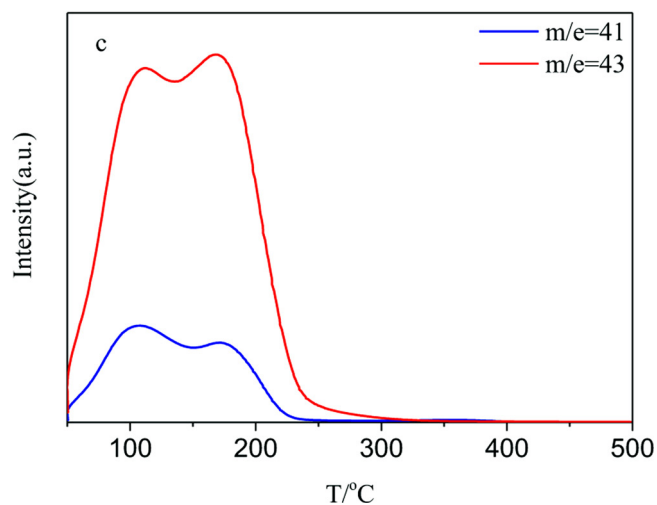
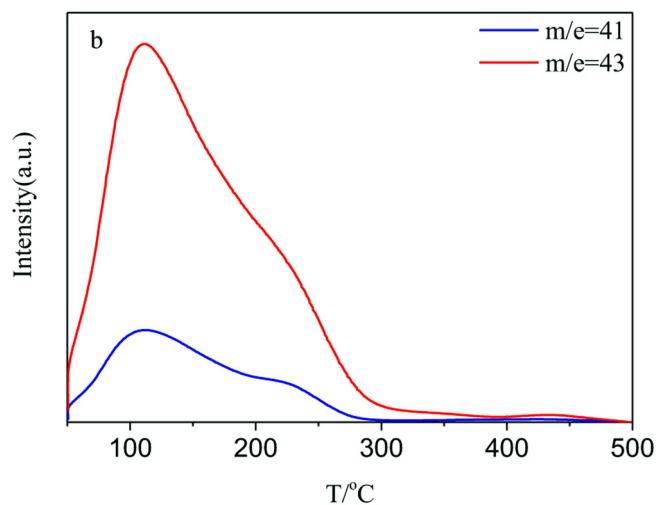
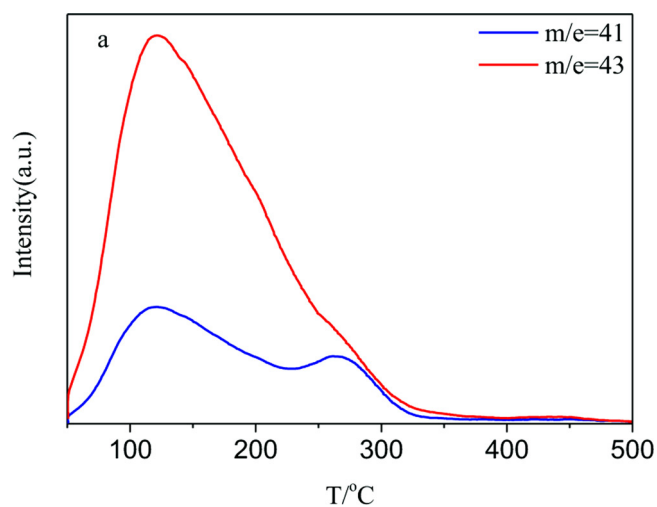


Fig. 9. IPA-TPD from ZnMgSi-X catalysts. (a, MgSi b, ZnMgSi-0.2 c, ZnMgSi-5).

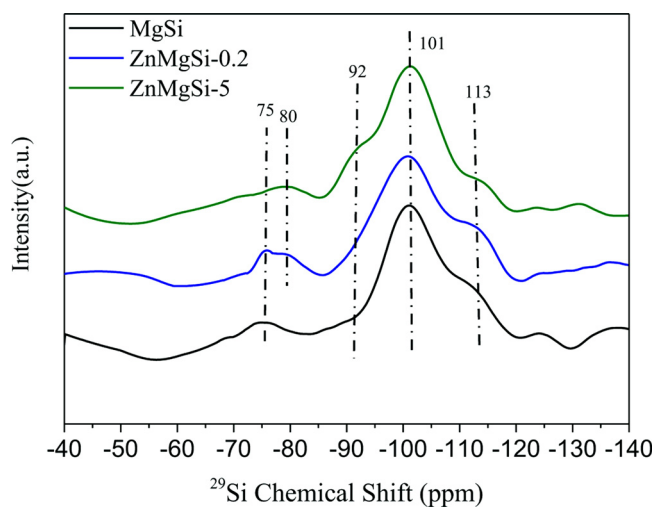


Fig. 10.  $^{29}\text{Si}$  MAS NMR patterns of the ZnMgSi-X catalysts.

Zn loading amounts, favoring a highly enhanced ethanol dehydrogenation capability and 1,3-BD yield due to the stronger surface basicity in Mg–O–Si interfacial structures, while the bulk ZnO species and the destruction of Mg–O–Si interfacial structures in the MgSi samples of higher Zn loading effectively suppressed the C–C bond growth and facilitated acetaldehyde production *via* ethanol dehydrogenation. The Mg–O–Si interfacial structures were shown to be the key structure-selectivity controller over product distribution.

#### CRediT authorship contribution statement

**Xuefei Wang:** Validation, Formal analysis, Investigation, Writing - original draft. **Yong Men:** Conceptualization, Methodology, Investigation, Writing - original draft. **Jinguo Wang:** Writing - review & editing. **Shuang Liu:** Writing - review & editing. **Qiaoling Song:** Validation. **Mei Yang:** Writing - original draft.

#### Declaration of Competing Interest

The authors declare that they have no known competing financial interests or personal relationships that could have appeared to influence the work reported in this paper.

#### Acknowledgments

This research was supported by the Talent Program of Shanghai University of Engineering Science, Science and Technology Commission of Shanghai Municipality (18030501100), National Natural Science Foundation of China (21503133, 21776274), Shanghai Talent Development Foundation (2017076) and the Program for Professor of Special Appointment (Eastern Scholar) at Shanghai Institutions of Higher Learning.

#### Appendix A. Supplementary data

Supplementary material related to this article can be found, in the online version, at doi:<https://doi.org/10.1016/j.apcata.2020.117565>.

#### References

- [1] C. Angelici, B.M. Weckhuysen, P.C. Bruijninx, *ChemSusChem* 6 (9) (2013) 1595–1614.
- [2] G.R. Dowson, M.F. Haddow, J. Lee, R.L. Wingad, D.F. Wass, *Angew. Chem. Int. Ed. Engl.* 52 (34) (2013) 9005–9008.
- [3] E.V. Makshina, M. Dusselier, W. Janssens, J. Degreve, P.A. Jacobs, B.F. Sels, *Chem. Soc. Rev.* 43 (22) (2014) 7917–7953.

- [4] J. Sun, Y. Wang, *ACS Catal.* 4 (4) (2014) 1078–1090.
- [5] R.J. Chimentão, J.E. Herrera, J.H. Kwak, F. Medina, Y. Wang, C.H.F. Peden, *Appl. Catal. A: Gen.* 332 (2) (2007) 263–272.
- [6] B. Chen, J. Lu, L. Wu, Z. Chao, *Chin. J. Catal.* 37 (11) (2016) 1941–1948.
- [7] I. Ro, Y. Liu, M.R. Ball, D.H.K. Jackson, J.P. Chada, C. Sener, T.F. Kuech, R.J. Madon, G.W. Huber, J.A. Dumesic, *ACS Catal.* 6 (10) (2016) 7040–7050.
- [8] V.L. Sushkevich, I.I. Ivanova, *Chemsuschem* 9 (16) (2016) 2216–2225.
- [9] H. Knözinger, R. Köhne, *J. Catal.* 5 (2) (1966) 264–270.
- [10] K. Ramesh, L.M. Hui, Y.-F. Han, A. Borgna, *Catal. Commun.* 10 (5) (2009) 567–571.
- [11] M. Timofeeva, *Appl. Catal. A: Gen.* 256 (1–2) (2003) 19–35.
- [12] S. Hanukovich, A. Dang, P. Christopher, *ACS Catal.* 9 (4) (2019) 3537–3550.
- [13] C.H. Christensen, B. Jorgensen, J. Rass-Hansen, K. Egeblad, R. Madsen, S.K. Klitgaard, S.M. Hansen, M.R. Hansen, H.C. Andersen, A. Riisager, *Angew. Chem. Int. Ed. Engl.* 45 (28) (2006) 4648–4651.
- [14] A.B. Sánchez, N. Homs, J. Fierro, P.R. de la Piscina, *Catal. Today* 107 (2005) 431–435.
- [15] M. Ni, D.Y. Leung, M.K. Leung, *Int. J. Hydrogen Energy* 32 (15) (2007) 3238–3247.
- [16] F. Romero-Sarria, J.C. Vargas, A.-C. Roger, A. Kiennemann, *Catal. Today* 133 (2008) 149–153.
- [17] M.C. Sanchez-Sanchez, R.M.N. Yerga, D.I. Kondarides, X.E. Verykios, J.L.G. Fierro, *J. Phys. Chem. A* 114 (11) (2010) 3873–3882.
- [18] W. Xu, Z. Liu, A.C. Johnston-Peck, S.D. Senanayake, G. Zhou, D. Stacchiola, E.A. Stach, J.A. Rodriguez, *ACS Catal.* 3 (5) (2013) 975–984.
- [19] J.D. McMillan, *Renew. Energy* 10 (2–3) (1997) 295–302.
- [20] A.D. Patel, K. Meesters, H. den Uil, E. de Jong, E. Worrell, M.K. Patel, *ChemSusChem* 6 (9) (2013) 1724–1736.
- [21] F. Liu, Y. Men, J. Wang, X. Huang, Y. Wang, W. An, *ChemCatChem* 9 (10) (2017) 1758–1764.
- [22] G.C. González, P. Concepción, A.V. Perales, A. Martínez, M. Campoy, F. Vidal-Barrero, *Fuel Process. Technol.* 193 (2019) 263–272.
- [23] G.C. González, R. Murciano, A.V. Perales, A. Martínez, F. Vidal-Barrero, M. Campoy, *Appl. Catal. A: Gen.* 570 (2019) 96–106.
- [24] C. Angelici, M.E. Velthoen, B.M. Weckhuysen, P.C. Bruijninx, *Catal. Sci. Technol.* 5 (5) (2015) 2869–2879.
- [25] S.-H. Chung, C. Angelici, S.O.M. Hinterding, M. Weingarth, M. Baldus, K. Houben, B.M. Weckhuysen, P.C.A. Bruijninx, *ACS Catal.* 6 (6) (2016) 4034–4045.
- [26] X. Huang, Y. Men, J. Wang, W. An, Y. Wang, *Catal. Sci. Technol.* 7 (1) (2017) 168–180.
- [27] S. Li, Y. Men, J. Wang, S. Liu, X. Wang, F. Ji, S. Chai, Q. Song, *Appl. Catal. A: Gen.* 577 (2019) 1–9.
- [28] C. Angelici, F. Meirer, A.M.J. van der Eerden, H.L. Schaink, A. Goryachev, J.P. Hofmann, E.J.M. Hensen, B.M. Weckhuysen, P.C.A. Bruijninx, *ACS Catal.* 5 (10) (2015) 6005–6015.
- [29] Y. Hayashi, S. Akiyama, A. Miyaji, Y. Sekiguchi, Y. Sakamoto, A. Shiga, T.R. Koyama, K. Motokura, T. Baba, *Phys. Chem. Chem. Phys.* 18 (36) (2016) 25191–25209.
- [30] C. Angelici, M.E. Velthoen, B.M. Weckhuysen, P.C. Bruijninx, *Chemsuschem* 7 (9) (2015) 2505–2515.
- [31] V.L. Dagle, M.D. Flake, T.L. Lemmon, J.S. Lopez, L. Kovarik, R.A. Dagle, *Appl. Catal. B: Environ.* 236 (2018) 576–587.
- [32] T. De Baerdemaeker, M. Feyen, U. Müller, B. Yilmaz, F.-S. Xiao, W. Zhang, T. Yokoi, X. Bao, H. Gies, D.E. De Vos, *ACS Catal.* 5 (6) (2015) 3393–3397.
- [33] R.A.L. Baylon, J. Sun, Y. Wang, *Catal. Today* 259 (2016) 446–452.
- [34] R. He, Y. Men, J. Liu, J. Wang, W. An, X. Huang, W. Song, J. Liu, S. Dai, *ChemCatChem* 10 (18) (2018) 3969–3973.
- [35] J. Sun, K. Zhu, F. Gao, C. Wang, J. Liu, C.H. Peden, Y. Wang, *J. Am. Chem. Soc.* 133 (29) (2011) 11096–11099.
- [36] C. Liu, J. Sun, C. Smith, Y. Wang, *Appl. Catal. A: Gen.* 467 (2013) 91–97.
- [37] W.E. Taifan, Y. Li, J.P. Baltrus, L. Zhang, A.I. Frenkel, J. Baltrusaitis, *ACS Catal.* 9 (1) (2018) 269–285.
- [38] W. Stöber, A. Fink, E. Bohn, *J. Colloid Interface Sci.* 26 (1) (1968) 62–69.
- [39] S. Kvisle, A. Aguero, R.P.A. Sneeden, *Appl. Catal.* 43 (1) (1988) 117–131.
- [40] P.B. Weisz, C.D. Prater, *Adv. Catal.* 6 (12) (1954) 143–196.
- [41] D.E. Mears, *Ind. Eng. Chem. Process. Des. Dev.* 10 (4) (1971) 541–547.
- [42] S.T. Oyama, X. Zhang, J. Lu, Y. Gu, T. Fujitani, *J. Catal.* 257 (1) (2008) 1–4.
- [43] S. Chai, Y. Men, J. Wang, S. Liu, Q. Song, W. An, G. Kolb, *J. CO<sub>2</sub> Util.* 33 (2019) 242–252.
- [44] E.V. Makshina, W. Janssens, B.F. Sels, P.A. Jacobs, *Catal. Today* 198 (1) (2012) 338–344.
- [45] O.V. Larina, P.I. Kyriienko, S.O. Soloviev, *Catal. Letters* 145 (5) (2015) 1162–1168.
- [46] T. Yan, L. Yang, W. Dai, C. Wang, G. Wu, N. Guan, M. Hunger, L. Li, *J. Catal.* 367 (2018) 7–15.
- [47] D. Dussol, N. Cadran, N. Laloue, L. Renaudot, J.-M. Schweitzer, *Chem. Eng. J.* (2020), <https://doi.org/10.1016/j.cej.2019.123586>.
- [48] B. Zhao, Y. Men, A. Zhang, J. Wang, R. He, W. An, S. Li, *Appl. Catal. A: Gen.* 558 (2018) 150–160.
- [49] H. Rajesh, U.S. Ozkan, *Ind. Eng. Chem. Res.* 32 (8) (1993) 1622–1630.
- [50] C.-I. Ahn, C. Kim, J.W. Bae, J. Jeon, H.S. Jung, Y.-B. Kim, S. Lee, J. Lee, K.-S. Ha, *Fuel Process. Technol.* 200 (2020) 106317.
- [51] K. Rintramee, K. Föttinger, G. Rupprechter, J. Wittayakun, *Appl. Catal. B* 115–116 (2012) 225–235.
- [52] R. He, Y. Men, X. Huang, J. Wang, S. Li, X. Wang, *Chem. Lett.* 47 (9) (2018) 1097–1100.
- [53] T. Tago, H. Konno, M. Sakamoto, Y. Nakasaka, T. Masuda, *Appl. Catal. A: Gen.* 403 (1–2) (2011) 183–191.
- [54] J.F. Stebbins, J.R. Smyth, W.R. Panero, D.J. Frost, *Am. Mineral.* 94 (7) (2009) 905–915.
- [55] Q. Zhu, B. Wang, T. Tan, *ACS Sustain. Chem. Eng.* 5 (1) (2016) 722–733.
- [56] J. Temuujin, K. Okada, K.J.D. Mackenzie, *J. Solid State Chem.* 138 (1) (1998) 169–177.
- [57] W. An, *J. Chem. Soc. Faraday Trans.* 17 (35) (2015) 22529–22532.
- [58] G. Li, S. Dissanayake, S.L. Suib, D.E. Resasco, *Appl. Catal. B: Environ.* 267 (2020), <https://doi.org/10.1016/j.apcatb.2019.118373>.